nature chemical biology

Supplementary information

https://doi.org/10.1038/s41589-024-01706-1

Engineered IscB–ωRNA system with expanded target range for base editing

In the format provided by the authors and unedited

Supplementary information

Supplementary Figures

Supplementary Fig. 1 | Functional properties of active IscB systems.

Supplementary Fig. 2 | Identification of TAM profiling.

Supplementary Fig. 3 | Secondary structures of ωRNA of IscB.m16 (a), IscB.m17 (b), IscB.m1 (c), IscB.m15 (d), and IscB.m18 (e) predicted by RNAfold.

Supplementary Fig. 4 | Substitutions of mismatched G-U or A-U to G-C based enhanced the EGFP fluorescence signal mediated by IscB.m16.

Supplementary Fig. 5 | Screening for variants with enhanced editing frequency using six GFxxFP reporters containing different TAMs.

Supplementary Fig. 6 | TAM recognitions of wild-type IscB.m16 and IscB.m16^{RESH} at 72 reporters.

Supplementary Fig. 7 | Translocation of IscB.m16*, enOgeuIscB and SpG Cas9 at VEGFA-S6 site in HEK293T cells.

Supplementary Fig. 8 | Introduction of D61A and/or H248A mutations results in nickase or abolished activity of IscB.m16 variants.

Supplementary Fig. 9 | A-to-G edits of IscB- and SpG-derived ABEs at endogenous sites in HEK293T cells.

Supplementary Fig. 10 | Indels of ABE and CBE systems.

Supplementary Fig. 11 | The gRNA-dependent off-target levels of SpG-ABE at predicted potential off-target sites.

Supplementary Fig. 12 | Domain architecture of different IscB.m16*-derived ABEs.

Supplementary Fig. 13 | The representative FACS gating strategy of IscB with non-target (NT, Left) and target sgRNA (Right).

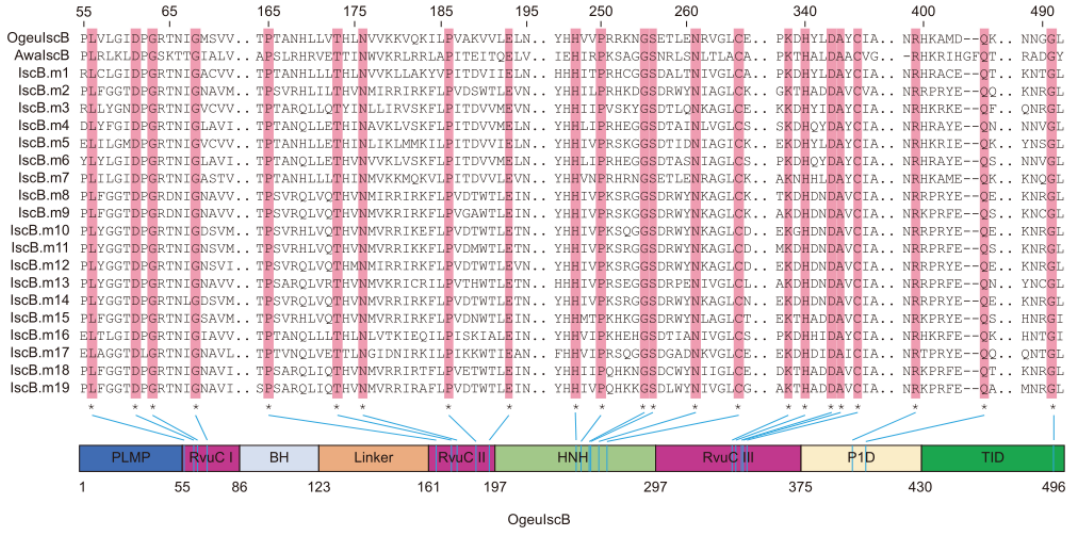

Supplementary Fig. 1 | Functional properties of active IscB systems. Distribution of conserved residues in 19 newly identified IscB proteins and 2 reported IscB proteins, OgeuIscB and AwaIscB. The conserved residues in RuvC, HNH, P1D and TID domains were marked as asterisks and blue lines in the bottom bar.

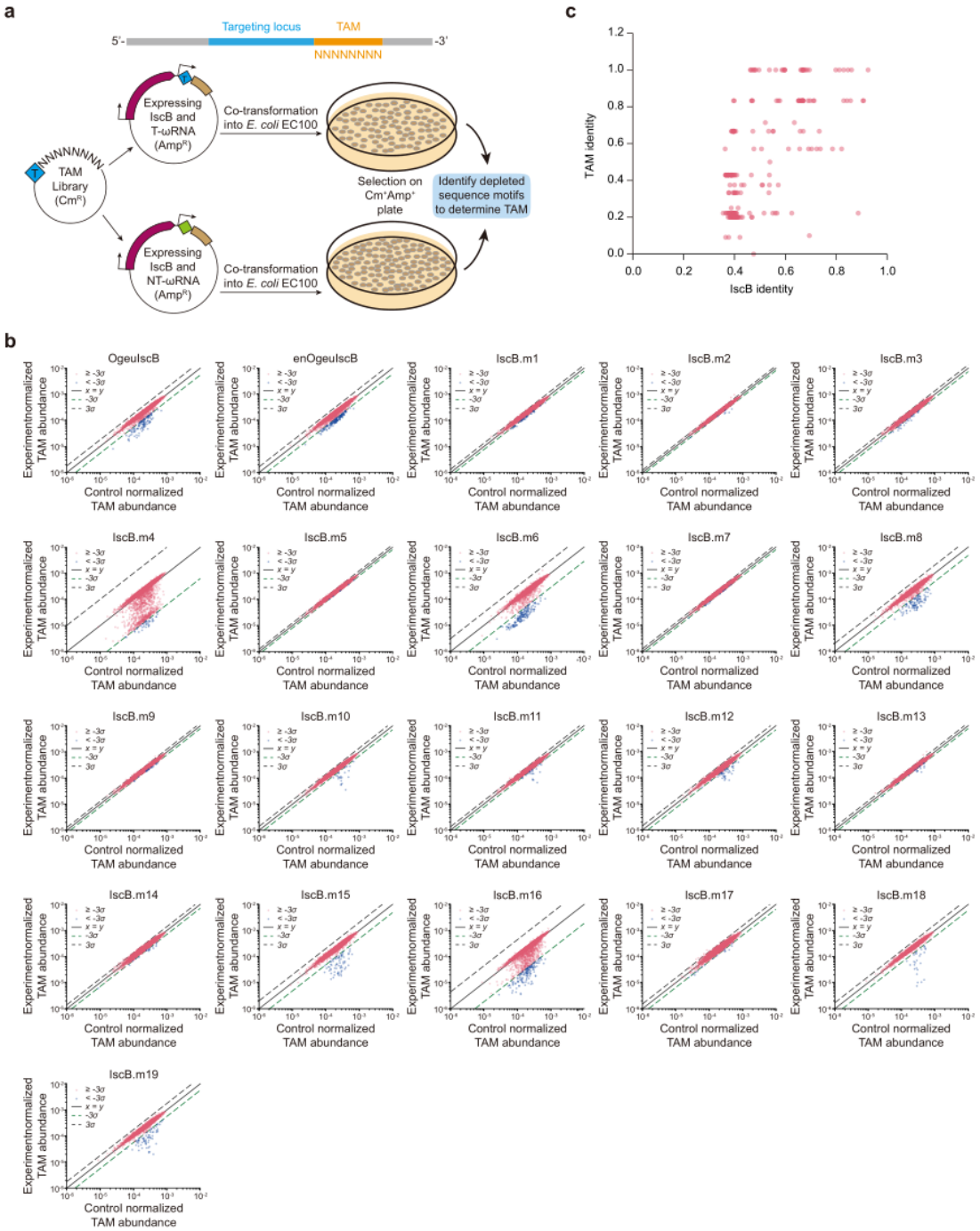

Supplementary Fig. 2 | Identification of TAM profiling. a, Schematic illustrating the plasmid depletion experiment for the detection of the TAM. **b,** Depletion data distribution plot of TAM profiling. Diagonal lines in coordinates represent that the ratio of experiment and control normalized TAM abundance is 1. σ means standard deviation (STD). Pink dots represent TAMs with over minus 3-fold STD, while blue dots denoting TAMs with less than minus 3-fold STD. **c,** The protein and TAM divergence plot of 19 active IscB proteins and OgeuIscB. The x-axis represents pairwise protein sequence divergence, and y-axis represents pairwise TAM divergence. A value close to 1 indicates high consistency, and close to 0 indicates high diversity.

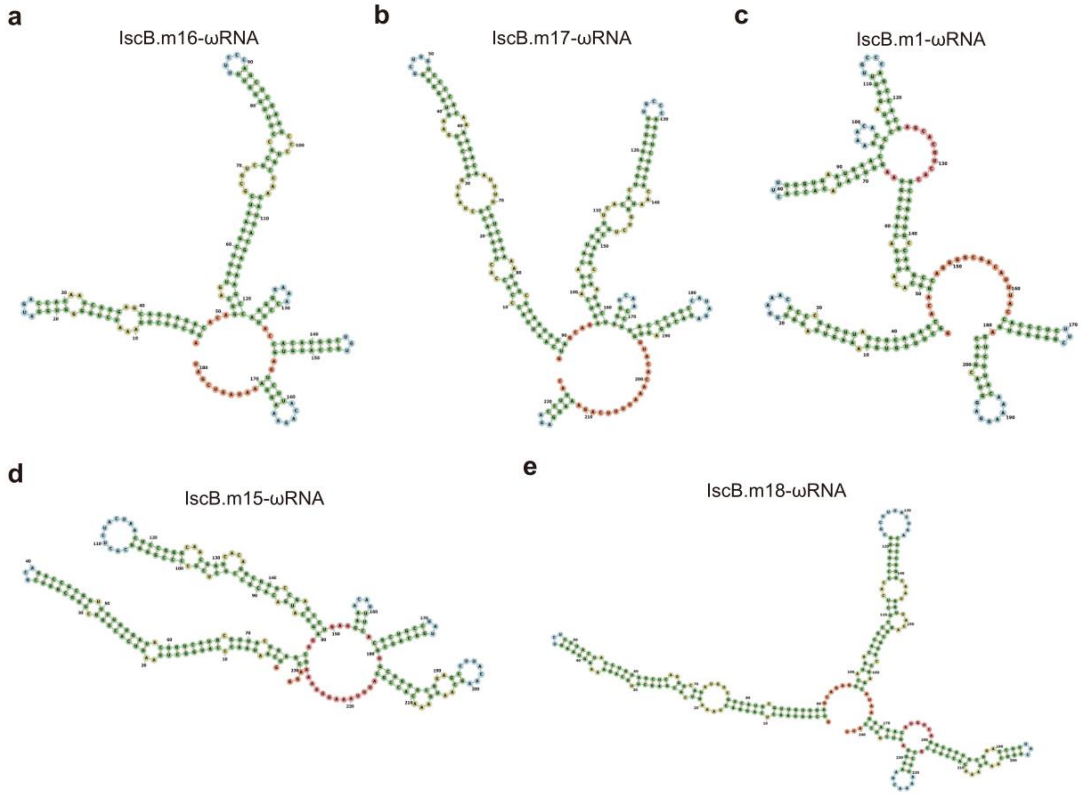

Supplementary Fig. 3 | Secondary structures of ωRNA of IscB.m16 (a), IscB.m17 (b), IscB.m1 (c), IscB.m15 (d), and IscB.m18 (e) predicted by RNAfold.

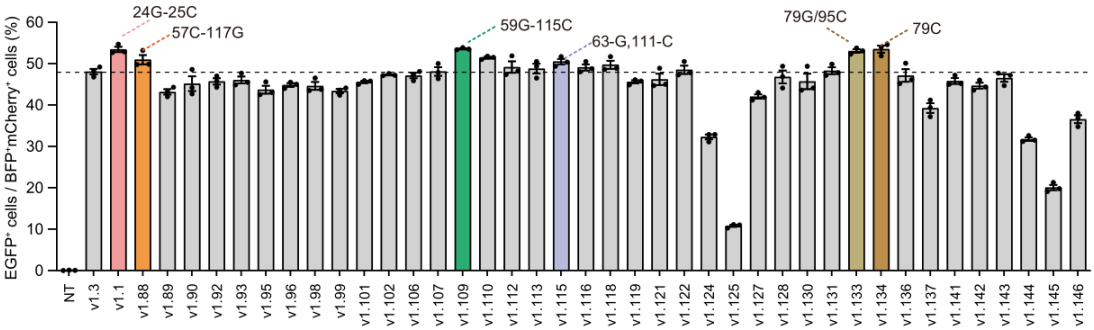

Supplementary Fig. 4 | Substitutions of mismatched G-U or A-U to G-C based enhanced the EGFP fluorescence signal mediated by IscB.m16. Data are exhibited as mean ± s.d., n = 3 independent biological replicates.

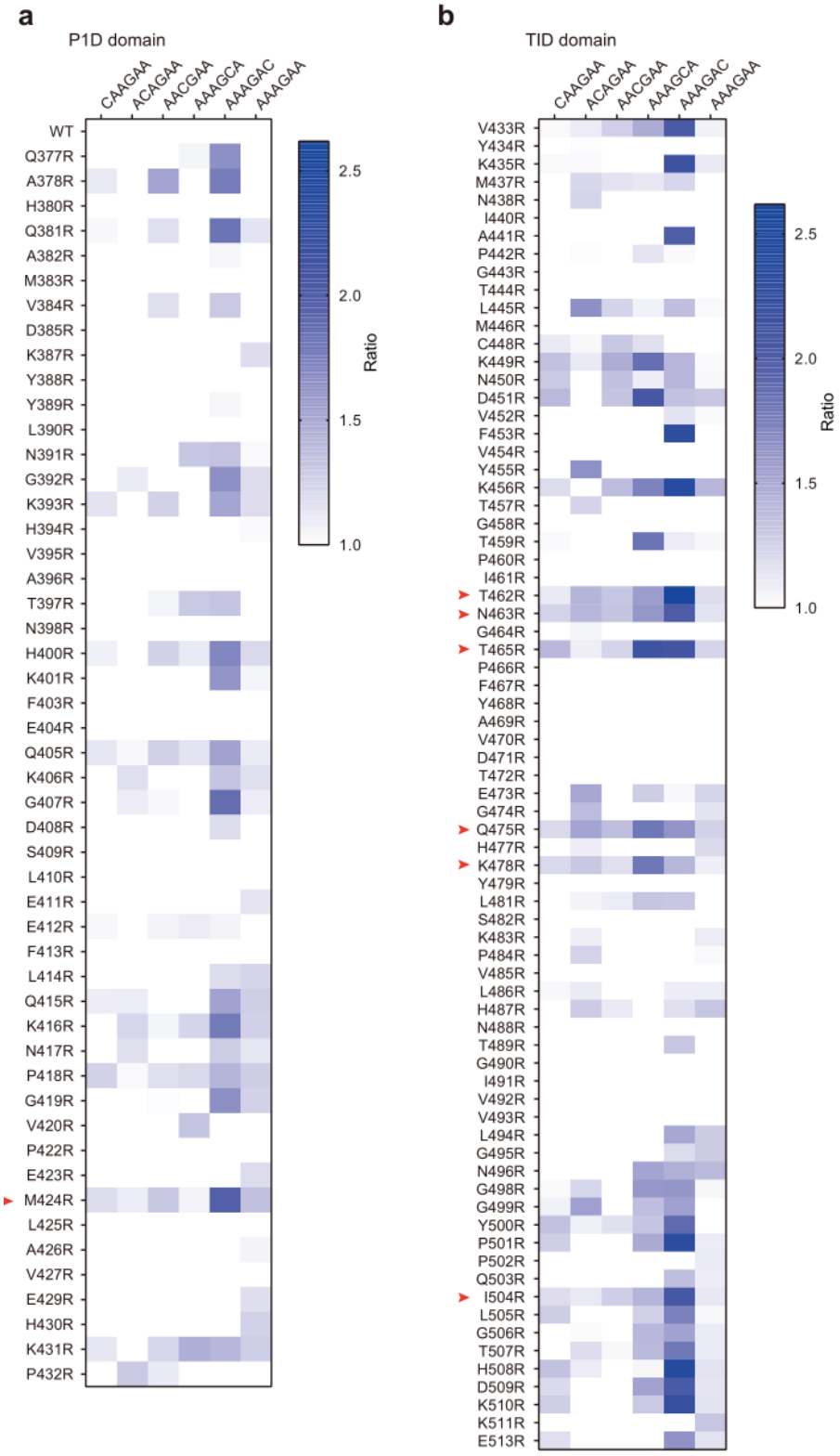

Supplementary Fig. 5 | Screening for variants with enhanced editing frequency using six GFxxFP reporters containing different TAMs. Substitutions of amino acid residues in P1D (**a**) and TID (**b**) domain of IscB.m16 protein with arginine. The shade of the color represents the ratio of the editing efficiency between WT IscB.m16 and its variants.

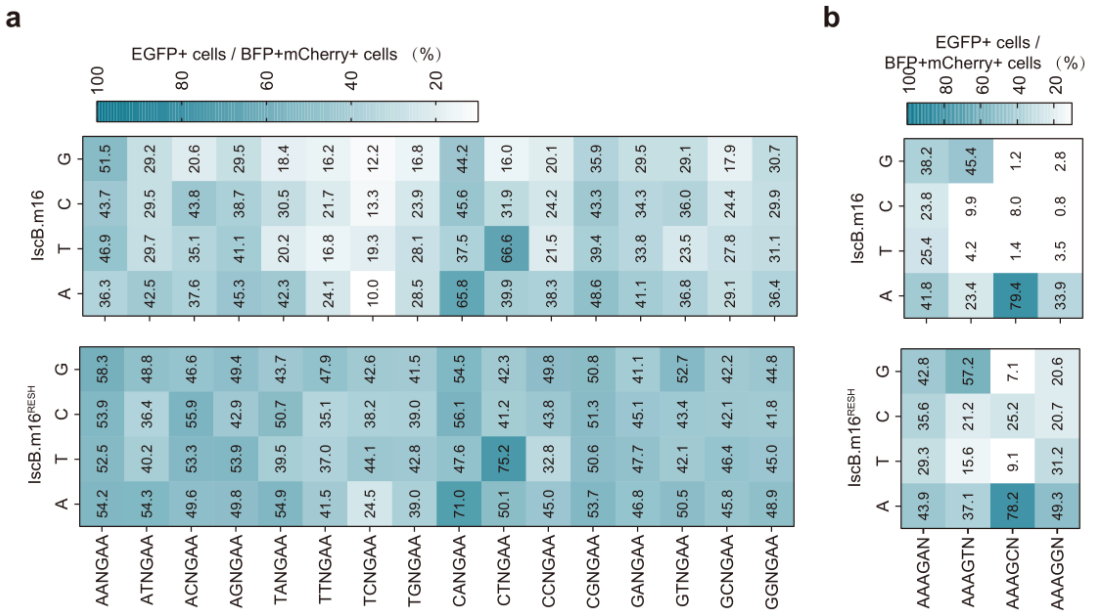

Supplementary Fig. 6 | TAM recognitions of wild-type IscB.m16 and IscB.m16^{RESH} at 72 reporters. a, Performance of two IscB.m16 variants at 64 reporters derived from 5'-NNNGAA-3', along with ωRNA-v2.27. **b,** Performance of two IscB.m16 variants at 16 reporters derived from 5'-AAAGNN-3', along with ωRNA-v2.27. Values represent mean of 3 independent biological replicates.

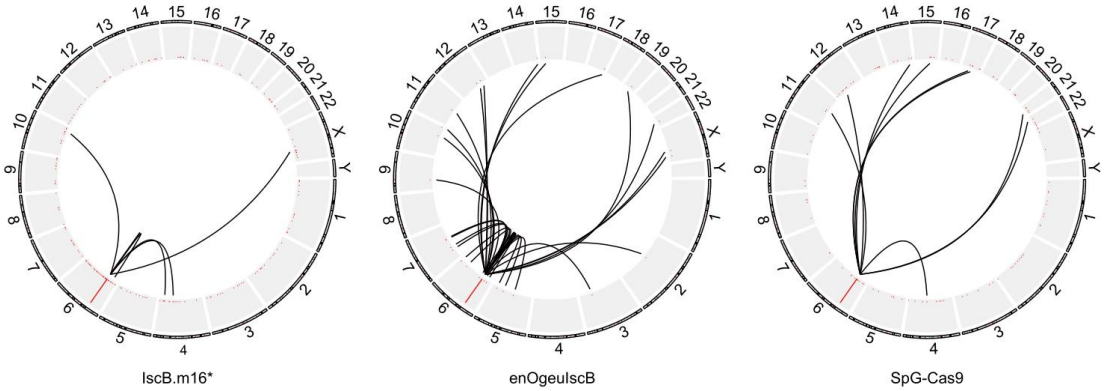

Supplementary Fig. 7 | Translocation of IscB.m16*, enOgeuIscB and SpG Cas9 at VEGFA-S6 site in HEK293T cells. Circos plot showing the genome-wide translocation events and the predicted off-target sites with translocation rate over 0.1% (the black lines linked to the target sites) of IscB.m16*, enOgeuIscB and SpG Cas9. The black lines only represent the distribution of high-frequency translocation sites, not the total translocation level.

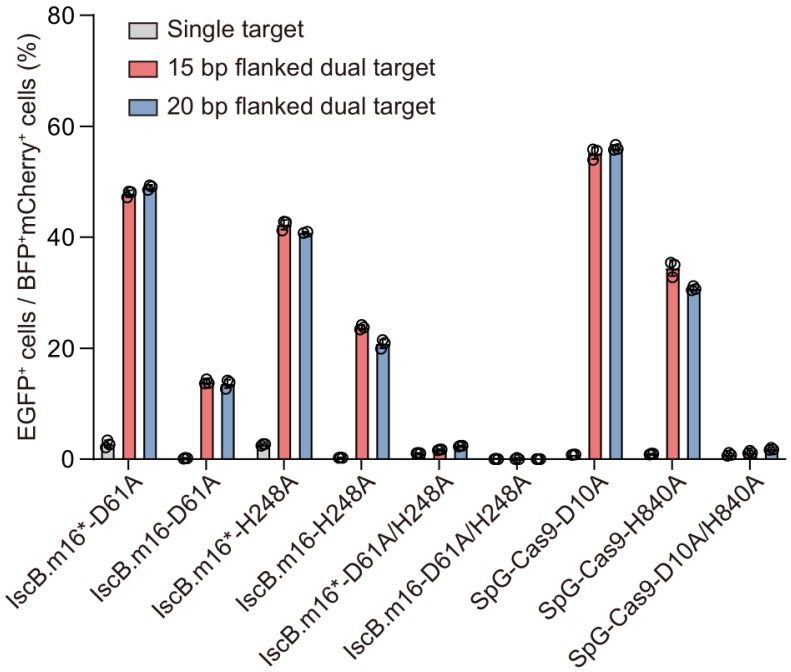

Supplementary Fig. 8 | Introduction of D61A and/or H248A mutations results in nickase or abolished activity of IscB.m16 variants. D10A and H840A mutations in SpCas9 serve as positive controls. Values and error bars were displayed as mean and s.d., n = 3 independent biological replicates.

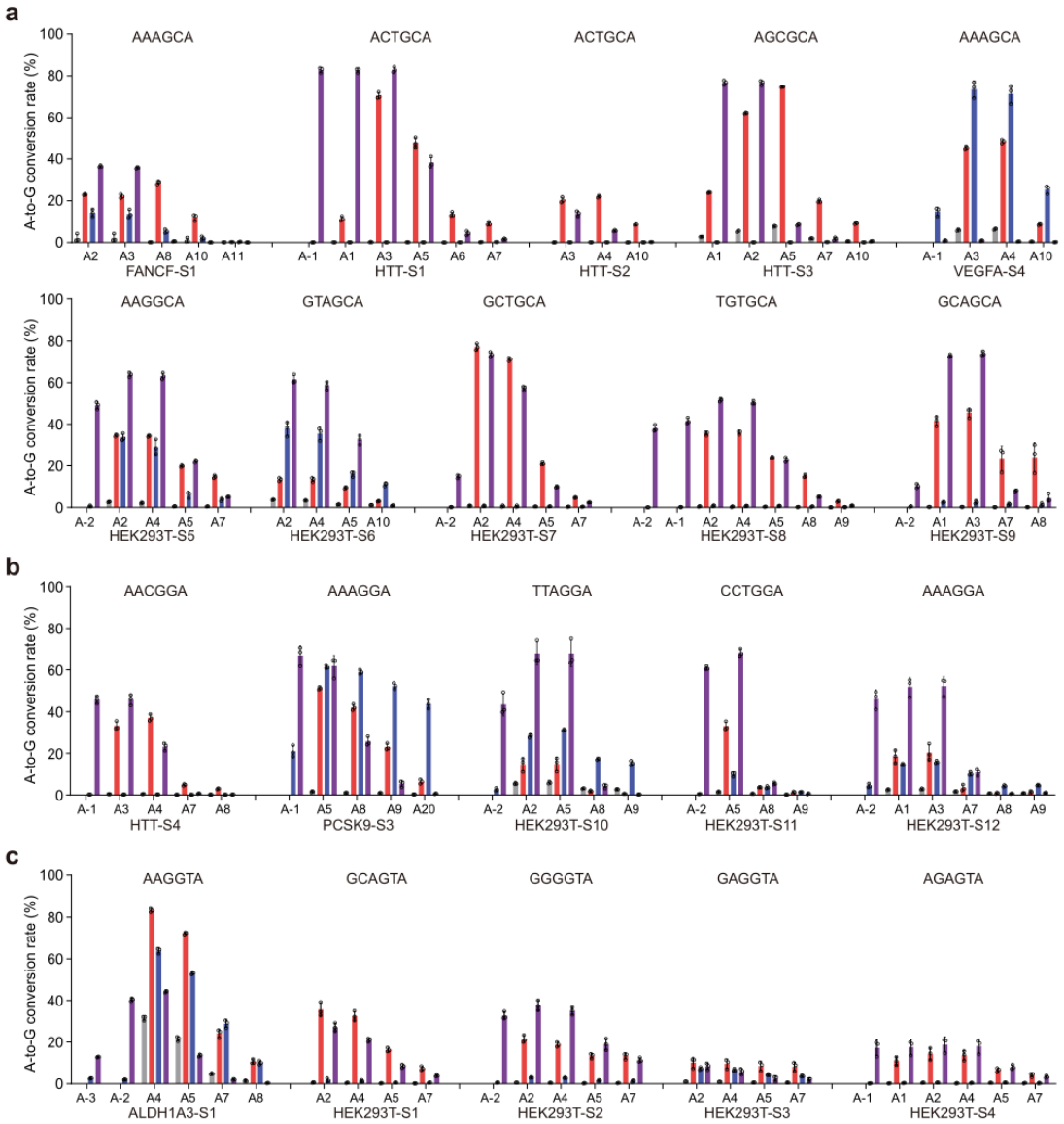

Supplementary Fig. 9 | A-to-G edits of IscB- and SpG-derived ABEs at endogenous sites in HEK293T cells. a-c, Comparisions of A > G conversion rate at 10 NNNGCA (**a**), 5 NNNGGA (**b**) and 5 NNNGTA TAMs sites (**c**), respectively. Data are exhibited as mean ± s.d., n = 3 independent biological replicates of each site.

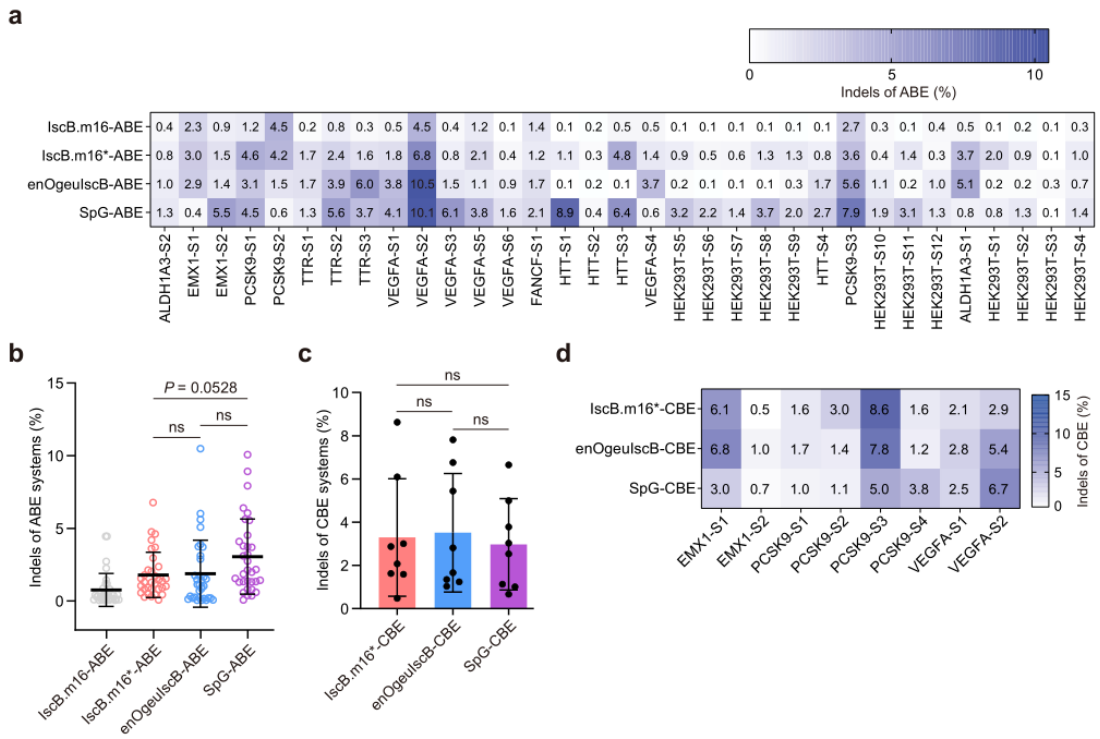

Supplementary Fig. 10 | Indels of ABE and CBE systems. a, Indels of four kinds of ABEs at 33 endogenous sites. Data are shown as mean of 3 independent biological replicates. **b,** Statistical analysis of indels generated by 4 kinds of ABEs at 33 endogenous loci respectively. Data are presented as mean ± s.d.. *P* values determined by Tukey's multiple comparisons test following ordinary one-way analysis of variance. NS, not significant. **c,** Statistical analysis of indels generated by 3 kinds of CBEs at 8 endogenous sites respectively. Values are shown as mean ± s.d.. Each dot represents mean indels of 3 independent biological replicates at one locus. *P* values determined by Tukey's multiple comparisons test following ordinary one-way analysis of variance. NS, not significant. **d,** Indels generated by 3 kinds of CBEs at 8 HEK293T sites. Values represent mean of 3 independent biological replicates at each site.

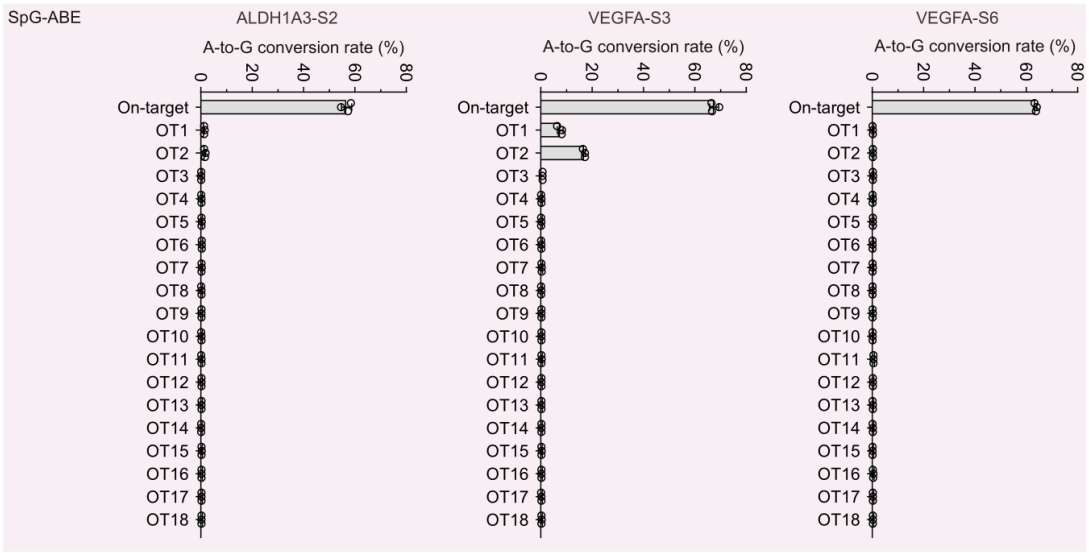

Supplementary Fig. 11 | The gRNA-dependent off-target levels of SpG-ABE at predicted potential off-target sites. Data are exhibited as mean ± s.d., n = 3 independent biological replicates.

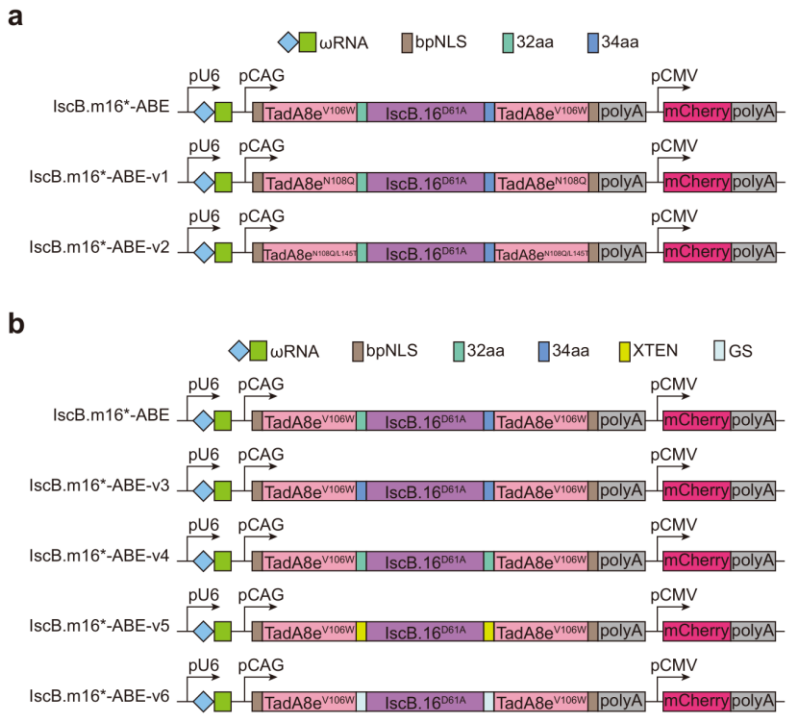

Supplementary Fig. 12 | Domain architecture of different IscB.m16*-derived ABEs. a, Different ABEs generated with different TadA8e variants. **b,** Different ABEs generated with different linkers.

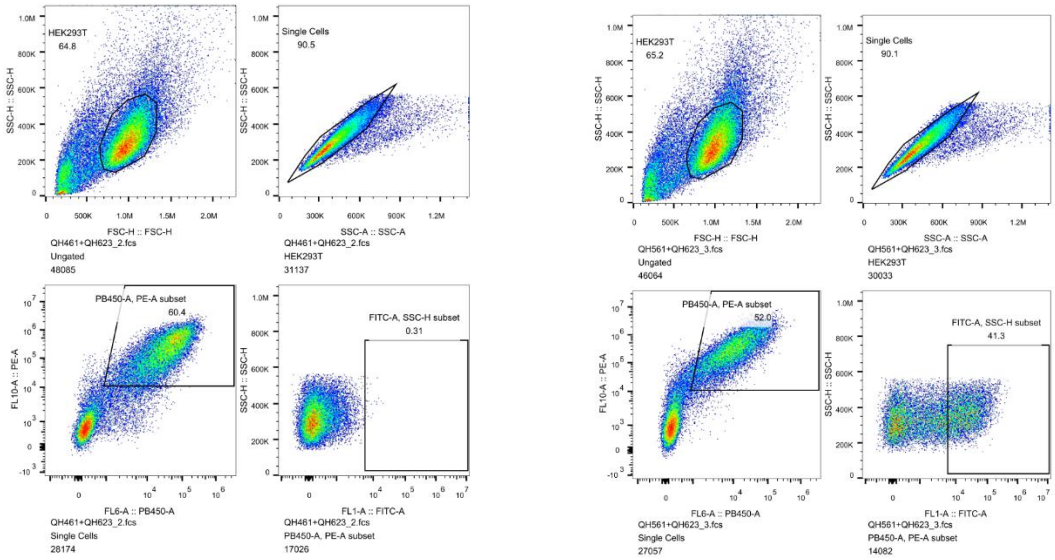

Supplementary Fig. 13 | The representative FACS gating strategy of IscB with non-target (NT, Left) and target sgRNA (Right).